Progress In Electromagnetics Research C, Vol. 66, 63–76, 2016

Single/Dual-Band BPFs with Spurious Band Suppression by Using Non-Uniform Coupled Resonators

Nagendra Kumar* **and Yatendra K. Singh**

Abstract—Transmission zero behavior of two coupled sections — interdigital and combline — is investigated. It is shown that the shifting of transmission zero of any coupled-section of a particular length depends on the width of various parts and the orientation of coupled-section. Mathematical formulation has been performed to show the effect of stepped discontinuity on the transmission zero. Further, this transmission zero allocation property is used in suppression of harmonics. The idea is implemented in two types of resonators — first in parallel-coupled resonators and second in open-loop resonators. Two parallel coupled resonator based bandpass filters (BPFs) with second harmonic suppression — one of second-order and the other of fourth-order — using different coupled-sections have been fabricated, and suppression up to −30 dB and −54 dB respectively has been achieved. A fourth-order open-loop resonators based BPF with suppression of undesired passbands up to $6.3f_o$ has been fabricated. Further, the above property is also used to design a dual-band BPF with wide stopband without increasing the size of the filter.

1. INTRODUCTION

Coupled resonators are the building block in designing microstrip BPFs. In past, these coupled resonators are configured in so many different ways to achieve filtering property, i.e., end-coupled configuration, edge- or parallel-coupled configuration [1], open-loop configuration [2], etc. Generally in all these configurations resonators are half wavelength ($\lambda_g/2$). Distributed nature of these $\lambda_g/2$ microstrip lines leads to spurious passbands unlike in lumped element-based filters. These spurious passbands results in selection of undesired channels in communication systems. So these undesired passbands must be suppressed or controlled.

Several techniques have been used to control or suppress the undesired passbands in the bandpass filters [3–12]. For example, an additional bandstop filter is cascaded with a bandpass filter to eliminate the spurious passbands at the cost of larger filter size and higher insertion loss [3]. In [4], wiggly-line structures are used to suppress spurious harmonic at $2f_o$ by modulating the wave impedance. The suppression of second harmonic can be achieved by creating periodic grooves in the resonators [5]. Fractal shaped filters are used in [6] to suppress second harmonic. Original transmission line is replaced with T-shaped lines to create the transmission zero at the second harmonic [7]. Suitable selection of coupling length leads to suppression of unwanted harmonics in [8]. Open-stubs are properly placed along with the open-loop resonators to achieve wide stopband as presented in [9]. Higher order harmonic suppression is also achieved by properly selecting the coupling region between shorted and open-loop resonators [10]. In [11], stepped impedance resonators (SIRs) are selected in such a way that they have the same fundamental resonating frequency but different spurious passband resonating frequencies, to achieve higher-order harmonic suppression. In [12] asymmetrical quarter-wavelength SIRs are used to suppress spurious harmonics.

Received 2 March 2016, Accepted 27 June 2016, Scheduled 16 July 2016
* Corresponding author: Nagendra Kumar (nagendra@iitp.ac.com).
The authors are with the Department of Electrical Engineering, Indian Institute of Technology Patna, 801103, India.

In [13], length of the coupling section is used to tune the transmission zero. In this paper, however, it is shown that the width of different parts and orientation of coupled section are the key factors in deciding the direction of tuning of transmission zeros created due to a particular coupled section of fixed length. Also, effects of stepped discontinuity on the transmission zeros are studied. This paper is organized as follows. Section 2 explains transmission zeros and their tuning associated with coupled-sections with different configurations. Mathematical analysis of these transmission zeros associated with the lumped parameters are discussed in Section 3. Section 4 deals with implementation of these transmission zeros in harmonic suppression. Filter design is discussed in Section 5. Sections 6 and 7 present the fabricated single and dual-band filters based on parallel-coupled resonators and open-loop resonators, respectively. A conclusion is given in 8.

2. COUPLED SECTIONS AND TRANSMISSION ZEROS

Figures 1(a) and 2(a) show the two widely used coupled sections — interdigital and combline — respectively. Fig. 1(a) shows the uniform coupled resonator with open ends on opposite sides, having width w and gap s. This uniform coupled resonator can be seen as consisting of three sections of uniform width. This coupled resonator is modified to stepped impedance coupled resonator having non-uniform width. Each stepped impedance coupled section consists of three equal-length sections having widths w_1, w_2 and w_3. Figs. 1(b) and 1(c) depict coupled resonator having different middle section widths, w_2, and corner section widths, w_3, respectively. In contrast to this Fig. 2(a) shows the coupled resonator having open-end on the same side with width w and gap s. Again this uniform coupled resonator is modified to achieve non-uniform coupled resonator as shown in Figs. 2(b) and 2(c).

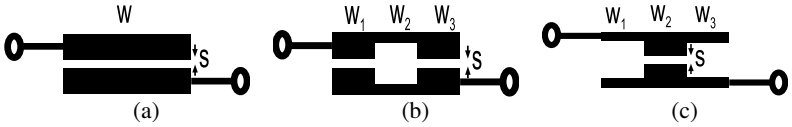

Figure 1. Interdigital coupled-section. (a) Uniform width. (b) Different middle width. (c) Different corner width.

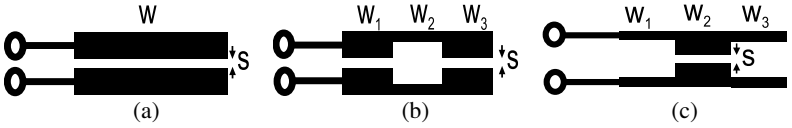

Figure 2. Combline coupled-section. (a) Uniform width. (b) Different middle width. (c) Different corner width.

The $ABCD$ parameter of the interdigital uniform coupled-section depicted in Fig. 1(a) can be written as [14]:

$$A = D = \frac{Z_{oe}\cot\theta_e + Z_{oo}\cot\theta_o}{Z_{oe}\csc\theta_e - Z_{oo}\csc\theta_o} \tag{1}$$

$$B = \frac{j}{2}\frac{Z_{oe}^2 + Z_{oo}^2 - 2Z_{oe}Z_{oo}(\cot\theta_e\cot\theta_o + \csc\theta_e\csc\theta_o)}{Z_{oe}\csc\theta_e - Z_{oo}\csc\theta_o} \tag{2}$$

$$C = \frac{2j}{Z_{oe}\csc\theta_e - Z_{oo}\csc\theta_o} \tag{3}$$

where θ_e and θ_o are even and odd-mode electrical lengths of coupled section, respectively. Z_{oe} and Z_{oo} are even and odd-mode impedances, respectively. Using above equations, S_{21} can be calculated as [14]:

$$S_{21} = \frac{2}{A + B/Z_o + CZ_o + D} \tag{4}$$

The frequency position of transmission zeros can be evaluated by equating $S_{21} = 0$ in Equation (4) and can be written as:

$$\frac{\csc\theta_e}{\csc\theta_o} = \frac{Z_{oo}}{Z_{oe}} \tag{5}$$

So on putting all physical parameters of a coupled section in Equation (5), frequencies of transmission zero are evaluated.

Similar type of mathematical analysis can be performed to find the frequency of transmission zeros of non-uniform coupled-sections shown in Figs. 1(b), 1(c), 2(a), 2(b), and 2(c).

According to Equation (5), transmission zero shifts to lower frequency as length increases and vice-verse. For a constant length l, effect of width w on the transmission zero is very small in uniform coupled resonator. But for a non-uniform or stepped impedance coupled resonator the effect of width of three sections cannot be ruled out. Further two coupled sections — interdigital and combline — of lengths $\lambda_{go}/4$ and $\lambda_{go}/8$ respectively are studied in Fig. 3 and Fig. 4, respectively. Throughout this paper, the substrate RT/Duroid 6010.2 with the relative dielectric constant of 10.2 having thickness of 0.635 mm is used for the simulation and measurement work.

Case A: S_{21} of interdigital coupled section depicted in Fig. 1(b), with respect to changing width w_2, is shown in Fig. 3(a). The length of coupled-section is $\lambda_{go}/4$. Transmission zeros associated with these types of coupled section shift to lower frequency as width of middle section, w_2, of coupled-section decreases. Interdigital coupled-sections of length $\lambda_{go}/4$, having uniform width, have a transmission zero after $2f_o$. So the transmission zero can be tuned to $2f_o$ by choosing appropriate width, w_2.

Case B: Fig. 3(b) shows the response S_{21} with respect to different w_1 ($w_1 = w_3$) for the layout shown in Fig. 1(c). In contrast to case A, in this case the first transmission zero shifts to higher frequency as the width decreases. Again the coupled-length is $\lambda_{go}/4$. Also the second transmission zero shifts to lower frequency. So this type of coupled-section is useful to suppress third and higher order harmonic. To suppress the second harmonic, length of the coupled section must be more than $\lambda_{go}/4$ such that transmission zero can be allocated near the second harmonic place.

Case C: In uniform $\lambda_{go}/8$ combline coupled-section, transmission zero comes just before $2f_o$. Fig. 4(a) shows the transmission zeros response with respect to different w_2 for the structure shown in Fig. 2(b). As width decreases, the first and second transmission zeros shift to higher and lower frequencies, respectively. So this combline coupled-section can be used to suppress two harmonics at a time by selecting appropriate width w_2.

Case D: Fig. 4(b) shows the response of the $\lambda_{go}/8$ length combline coupled-section shown in Fig. 2, with respect to different w_1 ($w_1 = w_3$). As width decreases the transmission zero shifts to $2f_o$.

Similar type of results can be plotted near $3f_o$ for $\lambda_{go}/6$ length interdigital coupled-section and $\lambda_{go}/12$ length combline coupled-section.

Basically decreasing or increasing width is related with the coupling between lines. So decrease in the middle section width, w_2, reduces the middle section coupling. Similarly, decrease in the last sections width reduces the end section coupling. So overall, coupling between different sections of the two coupled lines and the nature of arrangement — combline or interdigital — of these coupled lines decide the tuning of the transmission zeros.

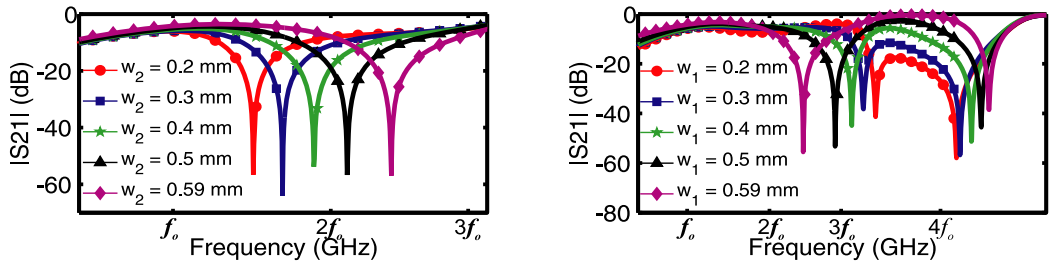

Figure 3. Response of the interdigital coupled-section (a) with changing w_2 ($w_1 = w_3 = 0.59$ mm, $s = 0.2$ mm), (b) with changing w_1 ($w_1 = w_3$, $w_2 = 0.59$ mm, $s = 0.2$ mm).

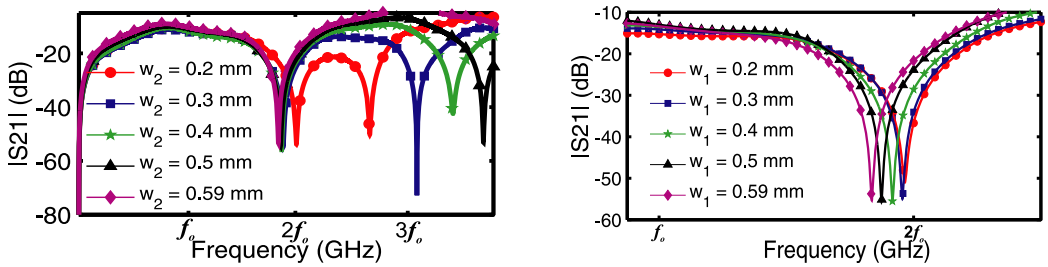

Figure 4. Response of the combline coupled-section (a) with changing w_2 ($w_1 = w_3 = 0.59\,\text{mm}$, $s = 0.2\,\text{mm}$), (b) with changing w_1 ($w_1 = w_3$, $w_2 = 0.59\,\text{mm}$, $s = 0.2\,\text{mm}$).

3. MATHEMATICAL ANALYSIS OF TRANSMISSION ZERO

The proposed coupled-structure includes steps in width. So for complete analysis of coupled section, this discontinuity must be included. The equivalent circuit at the stepped discontinuity of any microstrip transmission line is shown in Fig. 5(a) [15]. The equivalent circuit includes two inductors connected to micostrip line on either side and one capacitor to ground. Z_a and Z_b represent the impedances due to inductors L_1 and L_2, respectively. The impedances due to capacitors, C, are represented by Z_c. Fig. 5(b) shows the interdigital coupled-line having three sections with different widths and also includes the lumped equivalent circuit of discontinuities in width. In order to analyze the transmission zero associated with coupled-line, impedance parameters of the coupled-line are calculated. From Fig. 5, Z matrix for Section 1 can be written as:

$$\begin{bmatrix} V_1 \\ V_2 \\ V_3 \\ V_4 \end{bmatrix} = \begin{bmatrix} Z11^a & Z12^a & Z13^a & Z14^a \\ Z21^a & Z22^a & Z23^a & Z24^a \\ Z31^a & Z32^a & Z33^a & Z34^a \\ Z41^a & Z42^a & Z43^a & Z44^a \end{bmatrix} \begin{bmatrix} I_1 \\ I_2 \\ I_3 \\ I_4 \end{bmatrix} \tag{6}$$

Similarly, Z matrix for Section 2 can be written as:

$$\begin{bmatrix} V_5 \\ V_6 \\ V_7 \\ V_8 \end{bmatrix} = \begin{bmatrix} Z11^b & Z12^b & Z13^b & Z14^b \\ Z21^b & Z22^b & Z23^b & Z24^b \\ Z31^b & Z32^b & Z33^b & Z34^b \\ Z41^b & Z42^b & Z43^b & Z44^b \end{bmatrix} \begin{bmatrix} I_5 \\ I_6 \\ I_7 \\ I_8 \end{bmatrix} \tag{7}$$

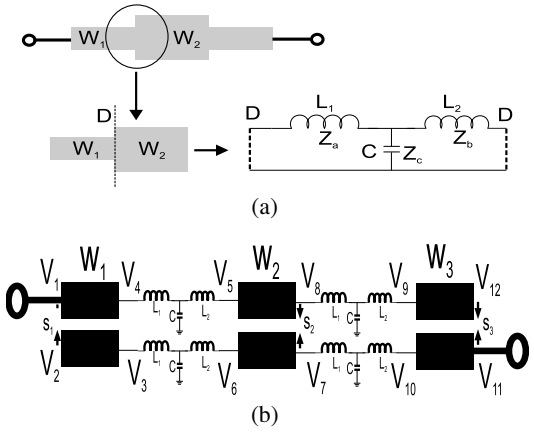

Figure 5. (a) Equivalent circuit of the step discontinuity. (b) Coupled line with step discontinuities.

and Z matrix for Section 3 with $w_1 = w_3$ can be written as:

$$\begin{bmatrix} V_9 \\ V_{10} \\ V_{11} \\ V_{12} \end{bmatrix} = \begin{bmatrix} Z11^a & Z12^a & Z13^a & Z14^a \\ Z21^a & Z22^a & Z23^a & Z24^a \\ Z31^a & Z32^a & Z33^a & Z34^a \\ Z41^a & Z42^a & Z43^a & Z44^a \end{bmatrix} \begin{bmatrix} I_9 \\ I_{10} \\ I_{11} \\ I_{12} \end{bmatrix} \tag{8}$$

The Z matrix of T-network of equivalent circuit of discontinuity can be represented as:

$$\begin{bmatrix} V_{4/3/8/7} \\ V_{5/6/9/10} \end{bmatrix} = \begin{bmatrix} Z11d & Z12d \\ Z21d & Z22d \end{bmatrix} \begin{bmatrix} -I_{4/3/8/7} \\ -I_{5/6/9/10} \end{bmatrix} \tag{9}$$

where $Z11d = Z_a + Z_c$, $Z22d = Z_b + Z_c$ and $Z12d = Z21d = Z_c$. Simplifying Equations (6)–(9), the complete matrix of coupled section can be written as (keeping port 2 and port 12 open for interdigital analysis):

$$\begin{bmatrix} V_1 \\ V_{11} \end{bmatrix} = \begin{bmatrix} Z11 & Z12 \\ Z21 & Z22 \end{bmatrix} \begin{bmatrix} I_1 \\ I_{11} \end{bmatrix} \tag{10}$$

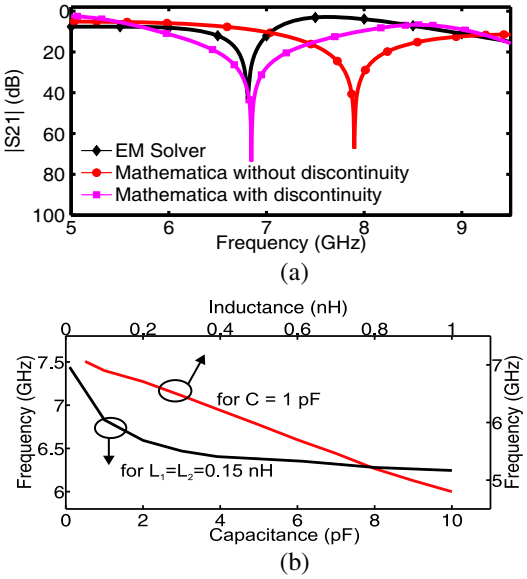

Figure 6. (a) Theoretical and simulated transmission zero response of a coupled-section. (b) Effect of discontinuity capacitors and inductors.

Further, the S-parameter of the coupled section is found in Mathematica [16] by above calculated Z-parameter using conversion formula described in [14]. Fig. 6(a) plots the the transmission zero of coupled section for the values $w_1 = w_3 = 0.2\,\text{mm}$, $w_2 = 0.59\,\text{mm}$, $s_1 = s_3 = 0.5\,\text{mm}$, $s_2 = 0.2\,\text{mm}$. As shown in Fig. 6(a), the position of transmission zeros without including discontinuity equivalent circuit has a mismatch with respect to solver result. Difference in the widths of two adjacent sections leads to change in the values of capacitors and inductors. In this specific case, the values of lumped components are $C = 1.0\,\text{pF}$ and $L_1 = L_2 = 0.15\,\text{nH}$. Fig. 6(b) shows the tuning of transmission zero with respect to the discontinuity capacitor and inductor. As inductance increases for the fixed value of the capacitance, transmission zero shifts to lower frequency. Similar conclusion can be drawn for the relation between the capacitance and transmission zero, although the absence of the equivalent circuit has no effect on the nature of the tuning of transmission zeros with respect to width of coupled-section. Similar to above, mathematical analysis for the other three cases of coupled sections can be performed.

4. PROPOSED RESONATOR AND HARMONIC SUPPRESSION

Figure 7 depicts the proposed non-uniform width resonator. The resonator used in the $\lambda_g/4$ interdigital coupled-section shown in Fig. 1(b) is depicted here for analysis. The resonator is $\lambda_g/2$ in length. It

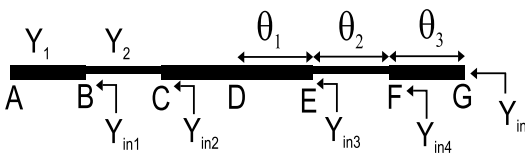

Figure 7. Proposed resonator.

consists of two different admittance microstrip lines Y_1 and Y_2. For simple calculation, a uniform electrical length, i.e., $\theta_1 = \theta_2 = \theta_3 = \theta$, is considered. The admittances of different sections, i.e., Y_{in1}, Y_{in2}, Y_{in3}, have been calculated to arrive at the final input admittance of the resonator, Y_{in}. The input admittance Y_{in} of the resonator can be written as:

$$Y_{in} = Y_1 \frac{Y_{in4} + jY_1 \tan\theta}{Y_1 + jY_{in4} \tan\theta} \tag{11}$$

By evaluating $Y_{in} = 0$, resonance condition of the proposed resonator can be written as:

$$\theta = \theta_o = \tan^{-1} \sqrt{\frac{Y_1 Y_2}{Y_1^2 + Y_1 Y_2 + Y_2^2}} \tag{12}$$

The other solutions can be written as [17]:

$$\theta_{s1} = \tan^{-1} \sqrt{\frac{Y_2(2Y_1 + Y_2)}{Y_1^2}} \tag{13}$$

$$\theta_{s2} = \pi/2 \tag{14}$$

$$\theta_{s3} = \pi - \theta_{s1} \tag{15}$$

$$\theta_{s4} = \pi - \theta_o \tag{16}$$

$$\theta_{s5} = \pi \tag{17}$$

Therefore, spurious frequency responses, f_{s1}, f_{s2}, f_{s3}, f_{s4}, f_{s5}, of the proposed resonator can be determined as:

$$\frac{f_{s1}}{f_o} = \frac{\tan^{-1} \sqrt{\frac{Y_2(2Y_1 + Y_2)}{Y_1^2}}}{\tan^{-1} \sqrt{\frac{Y_1 Y_2}{Y_1^2 + Y_1 Y_2 + Y_2^2}}} \tag{18}$$

$$\frac{f_{s2}}{f_o} = \frac{\pi}{2\tan^{-1} \sqrt{\frac{Y_1 Y_2}{Y_1^2 + Y_1 Y_2 + Y_2^2}}} \tag{19}$$

$$\frac{f_{s3}}{f_o} = 2\frac{f_{s2}}{f_o} - \frac{f_{s1}}{f_o} \tag{20}$$

$$\frac{f_{s4}}{f_o} = 2\frac{f_{s2}}{f_o} - 1 \tag{21}$$

$$\frac{f_{s5}}{f_o} = 2\frac{f_{s2}}{f_o} \tag{22}$$

Similar to this, design equations for other resonators can also be achieved.

For wider stopband these harmonics need to be suppressed. The transmission zeros of the resonator are relocated by changing the width at the position of the above harmonics to suppress them. As discussed above, for interdigital coupled section of length $\lambda_{go}/4$, the transmission zero is positioned after $2f_o$. So to suppress spurious passband at $2f_o$, coupled section is modified to that of Case A so

that transmission zero shifts to the position of undesired passband. If Case B coupled section is used, then it is easy to suppress the third harmonic. But to suppress the second harmonic, the coupled-length must be increased. Similarly, a open-loop resonator is introduced to use combline coupled-section. To suppress more than one harmonics, multiple coupled-sections are required. So higher-order filters can suppress more than one harmonics at a time. To design the filter, coupled-length (for case B coupled-section only) and the width associated with these coupled-sections must be selected using EM solver or Mathematica. Length of coupled-part and the width are selected according to the position of harmonic suppression. One important point to be noted is that there is a slight change in the center frequency due to the change in the coupled width.

5. COUPLING COEFFICIENT AND EXTERNAL QUALITY FACTOR

In this paper, element values of the low-pass prototype having Chebyshev response are used in all the cases. From the given low-pass prototype element values, two important design parameters — external quality factors and coupling coefficients — can be calculated as follows [15]:

$$Q_{ei} = \frac{g_0 g_1}{FBW} \tag{23}$$

$$Q_{eo} = \frac{g_n g_n + 1}{FBW} \tag{24}$$

$$M_{i,i+1} = \frac{FBW}{\sqrt{g_i g_{i+1}}}, \quad \text{for i} = 1 \text{ to } n-1 \tag{25}$$

where Q_{ei} and Q_{eo} are the external quality factors of the resonators at the input and output, respectively, and $M_{i,i+1}$ is the coupling coefficient between the ith and $(i+1)$th resonators. The FBW is the abbreviation for fractional bandwidth. Full wave simulator High Frequency Structure Simulator (HFSS) [18] is used to extract quality factor and coupling coefficient. From the simulator, coupling coefficient can be evaluated by two dominant resonant frequencies f_p and f_q as [15]:

$$M_{i,i+1} = \frac{f_p^2 - f_q^2}{f_p^2 + f_q^2}. \tag{26}$$

So this equation guides the selection of a proper coupling gap between the resonators according to the required coupling-coefficient. From simulation, the external quality factor can be determined as [15]:

$$Q_e = \frac{\omega_o}{\Delta\omega_{\pm 90^\circ}} \tag{27}$$

where ω_o is the resonating frequency, and $\Delta\omega_{\pm 90^\circ}$ is the absolute bandwidth between the $\pm 90^\circ$ points on the phase plot of S_{11} relative to its phase at ω_o. In this paper, 0° tapped feed is used to design all filters so that better selectivity can be achieved [19]. The above calculated quality factor determines the tapping position.

6. PARALLEL-COUPLED RESONATOR BASED BANDPASS FILTER DESIGN

Based on the above analysis, harmonic-suppressed BPFs are designed. HFSS is used to analyze the filters. The filters are fabricated on a substrate RT/Duroid 6010.2 with the relative dielectric constant of 10.2, thickness of 0.635 mm and loss tangent of 0.0023. The responses of the fabricated filters are measured by an Agilent E5071C network analyzer.

6.1. Fourth-Order BPF with Second Harmonic Suppression Using Case A Coupled-Section

A fourth-order parallel-coupled type BPF consisting of interdigital open-ended resonators is designed and fabricated with center frequency of 2.27 GHz having FBW of 0.19 or 19%. Fig. 8 shows the layout of the BPF. Case A is used as the coupled-section to suppress the second harmonic. The lumped circuit element values of the Chebyshev low-pass prototype filter with a passband ripple of 0.18 dB are $g_0 = 1$,

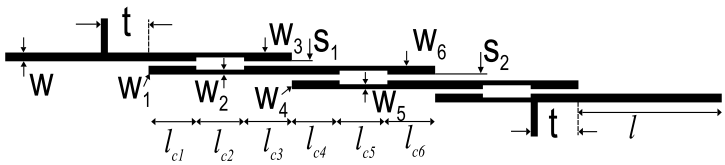

Figure 8. Layout of a fourth-order parallel-coupled BPF.

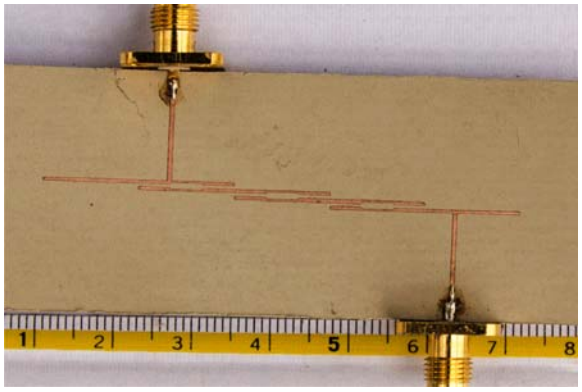

Figure 9. Fourth-order parallel-coupled BPF. (a) Fabricated filter. (b) Simulated and measured performance of the filter with the second harmonic suppression. (c) Group delay.

$g_1 = 1.2698$, $g_2 = 1.2901$, $g_3 = 1.9412$ and $g_4 = 0.8439$ and $g_5 = 1.5047$. The input/output external quality factors and coupling coefficients can be evaluated as:

$$Q_{ei} = Q_{eo} = \frac{g_0 g_1}{FBW} = 6.683$$

$$M_{12} = M_{34} = \frac{FBW}{\sqrt{g_1 g_2}} = 0.1485$$

$$M_{23} = \frac{FBW}{\sqrt{g_2 g_3}} = 0.1201.$$

This gives the tapping position $t = 3.8\,\text{mm}$ and the gap between the resonators $s_1 = 0.28\,\text{mm}$ and $s_2 = 0.35\,\text{mm}$ by using Equations (27) and (26), respectively. Fig. 9(a) depicts the fabricated fourth-order BPF having suppressed second harmonic. The dimensions of the fabricated BPF are $l_{c1} = l_{c2} = l_{c3} = 4.0\,\text{mm}$, $l_{c4} = l_{c5} = l_{c6} = 4.0\,\text{mm}$, $w_1 = w_3 = w = 0.59\,\text{mm}$, $w_4 = w_6 = 0.59\,\text{mm}$, $w_2 = w_5 = 0.2\,\text{mm}$, and $l = 12\,\text{mm}$. The simulation and measurement results of the fourth-order filter are displayed in Fig. 9(b). The response shows two transmission zeros on either side of passband due to 0° feed. The response shows a insertion loss of 2.55 dB. Also rejection of 54 dB has been achieved at the second harmonic position. A group delay less than 3.8 ns has been achieved within the passband of the fabricated BPF as depicted in Fig. 9(c).

6.2. Second-Order BPF with Second Harmonic Suppression Using Case B Coupled-Section

Filter design using case B type of coupled-section requires more coupled length to suppress the second harmonic because the transmission zero shifts to higher frequency when corner width decreases. The second-order parallel-coupled Chebyshev BPF having FBW of 10% centered at 2.24 GHz with 0.2 dB ripple level is designed and fabricated. Case B type of coupled-section is used for suppression of second harmonic. The element values of the Chebyshev low-pass prototype filter are $g_0 = 1$, $g_1 = 1.0379$, $g_2 = 0.6746$ and $g_3 = 1.5386$. The input/output external quality factors and coupling coefficients can be evaluated as:

$$Q_{ei} = Q_{eo} = \frac{g_0 g_1}{FBW} = 10.4$$

$$M_{12} = \frac{FBW}{\sqrt{g_1 g_2}} = 0.12.$$

The tapping position and the gap between the resonators are found as $t = 3$ mm and $s_1 = 0.7$ mm respectively by using Equations (27) and (26). Fig. 10(a) shows the layout of the filter. The dimensions of the fabricated second-order BPF are $l_{c1} = 4.0$ mm, $l_{c2} = 10.0$ mm, $l_{c3} = 4.0$ mm, $w_1 = w_3 = 0.2$ mm, $w_2 = w = 0.59$ mm, $l = 6$ mm. The response of the BPF is shown in Fig. 10(b). The suppression at the second harmonic is up to -30 dB. The fabricated BPF shows a insertion loss of 0.77 dB. The first and second transmission zeros of the coupled resonators come at 4.0 GHz and 4.75 GHz, respectively, near the second harmonic position, which increase the rejection capability of the BPF as discussed in Fig. 3(b). The group delay within the passband of the BPF is less than 1.95 ns as plotted in Fig. 10(c).

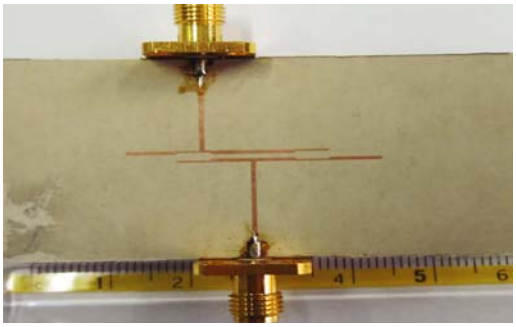

(a)

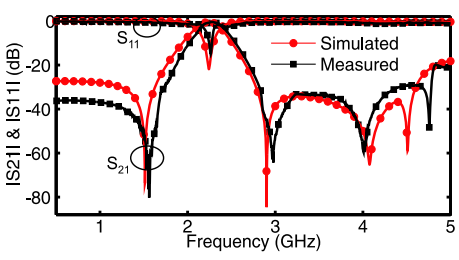

(a)

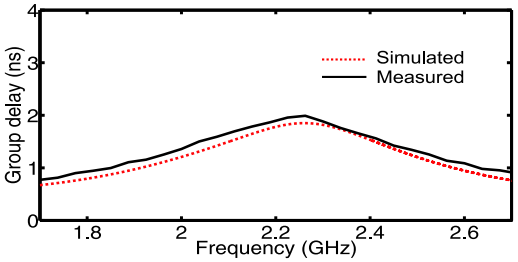

(c)

Figure 10. Second-order parallel-coupled BPF. (a) Layout. (b) Simulated and measured performance of the filter with the second harmonic suppression. (c) Group delay.

In a similar fashion, other higher-order filters can be designed with more higher-order harmonics suppression.

7. OPEN-LOOP RESONATOR BASED BPF DESIGN

7.1. Second-Order BPF with Second and Third Harmonic Suppression

To show the application of the changing width in combline coupled section open-loop resonators based BPF is designed. The layout of second-order filter is depicted in Fig. 11(a). To retain the combline property, open-loop resonators are coupled in such a way so that both open ends are on the same side. Also Case C is used to design the coupled part. As discussed in Section 2, this type of coupled section is able to suppress two harmonics at a time. Fig. 11(b) plots the S_{21} for the second order BPF for two different values of w_2. When the width $w_2 = 0.4\,\text{mm}$, suppression of $-20\,\text{dB}$ has been achieved up to the second harmonic. But at $w_2 = 0.2\,\text{mm}$, the first and second transmission zeros associated with the coupled parts are correctly placed near the second and third harmonic positions respectively, which leads to the suppression of $-20\,\text{dB}$ up to $4f_o$. So by changing the width, two harmonics are suppressed simultaneously without changing the coupled-length. The dimensions used for both the simulations are $l_{c1} = 2.0\,\text{mm}$, $l_{c2} = 2.0\,\text{mm}$, $l_{c3} = 2.4\,\text{mm}$, $w_1 = w_3 = w = 0.59\,\text{mm}$. Quality factor and coupling-coefficient must be maintained while changing the coupled section width.

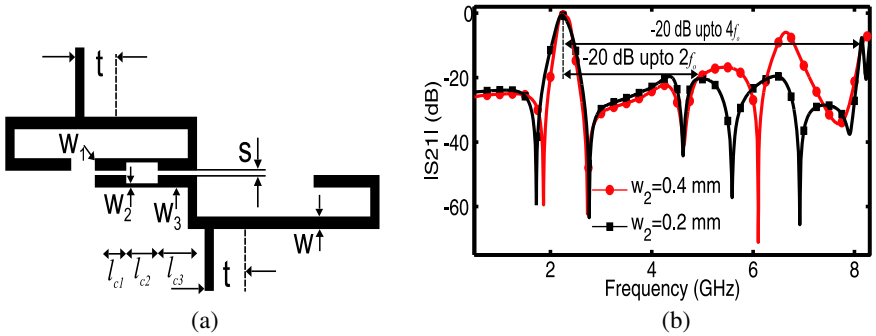

Figure 11. Second-order open-loop BPF. (a) Layout. (b) Simulated performance with the second and third harmonic suppression at different w_2.

7.2. Fourth-Order BPF with Second, Third and Fourth Harmonic Suppression

A fourth-order BPF consisting of open-loop resonator is designed and fabricated. A fourth-order BPF has three coupled-lengths. The schematic of the BPF is depicted in Fig. 12. The first and last coupled-sections are used to suppress the second harmonic, and the middle coupled-section is used to suppress the third and fourth harmonics both at the same time. So the property of Case C is used to suppress two harmonics at a time. The fourth-order Chebyshev BPF is designed with a 0.05-dB ripple level and 9.5% FBW at the center frequency of 2.27 GHz. The lumped circuit element values of the low-pass prototype filter are $g_0 = 1$, $g_1 = 0.9588$, $g_2 = 1.2970$, $g_3 = 1.6078$ and $g_4 = 0.7735$ and $g_5 = 1.2396$. The input/output external quality factors and coupling coefficients can be evaluated as:

$$Q_{ei} = Q_{eo} = \frac{g_0 g_1}{FBW} = 10.1$$

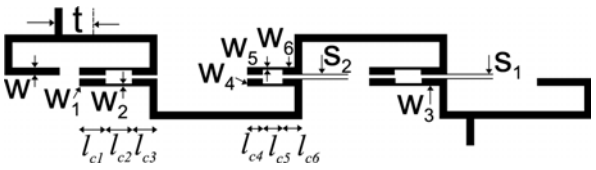

Figure 12. Layout of a fourth-order open-loop BPF.

$$M_{12} = M_{34} = \frac{FBW}{\sqrt{g_1 g_2}} = 0.0852$$
$$M_{23} = \frac{FBW}{\sqrt{g_2 g_3}} = 0.0658.$$

This determines the tapping position $t = 3.25\,\text{mm}$ and the gap between the resonators $s_1 = 0.25\,\text{mm}$, $s_2 = 0.28\,\text{mm}$, by using Equations (27) and (26). To suppress the second, third and fourth harmonics, the required coupling lengths of the first and second coupled sections will be near $\lambda_{go}/8$ and $\lambda_{go}/12$, respectively. The dimensions of the proposed filter are $l_{c1} = l_{c2} = 2\,\text{mm}$, $l_{c3} = 2.58\,\text{mm}$, $l_{c4} = l_{c5} = 1.5\,\text{mm}$, $l_{c6} = 1.8\,\text{mm}$, $d = 1.5\,\text{mm}$, $w_1 = w_3 = w = 0.59\,\text{mm}$ and $w_2 = 0.2\,\text{mm}$. The fabricated fourth-order BPF and its responses are shown in Fig. 13. The insertion loss of the fabricated BPF is 1.68 dB. The suppressions at the second, third and fourth harmonics are up to −39 dB. In addition to this, a wide stopband up to $6.3f_o$ at the level of −24 dB is also achieved. The group delay of the fabricated BPF is depicted in Fig. 13(c). Within the passband, a group delay of 6.0 ns is attained. Also Table 1 compares this work with the previous reported works.

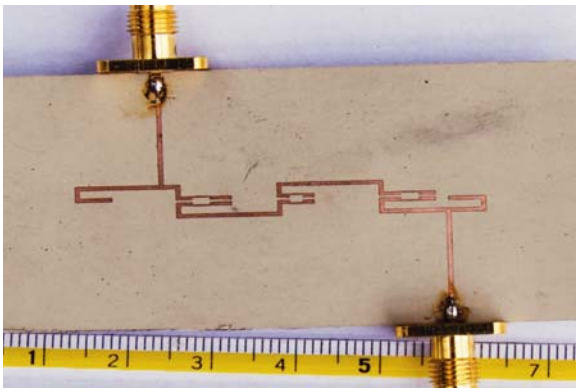

(a)

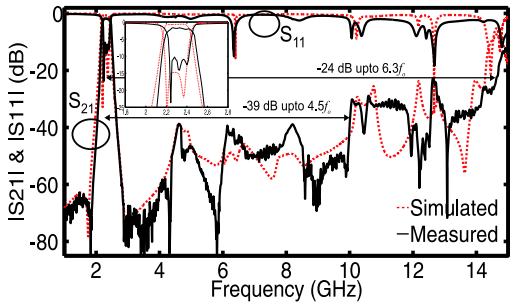

(b)

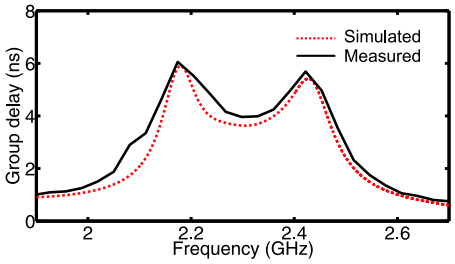

(c)

Figure 13. Fourth-order open-loop BPF. (a) Fabricated filter. (b) Measured and simulated performance of the filter with higher-order suppression. (c) Group delay.

7.3. Dual-Band BPF with Harmonic Suppression

The proposed concept of harmonic suppression can be further extended to dual-band BPF. Fig. 14(a) depicts the schematic of a dual-band BPF using stub-loaded open-loop resonators, where Z_1, L_1, Z_s and L_s represent the characteristic impedances and the lengths of the open-loop line and open-stub, respectively. The open-stub is connected at the middle of the open-loop line. Now the odd and even-mode analysis can be used to define the resonance frequencies of the symmetrical structure. By odd-

Table 1. Comparison with the previous reported works.

Ref.	Cent.freq. f_o (GHz)	Size λ_o^2	Insert. loss (dB)	Stopband suppression level
[10]	0.97	0.14×0.073	0.9	20 dB up to $4f_o$
[11]	1.5	0.59×0.14	2.9	30 dB up to $5.4f_o$
[12]	1.5	0.16×0.12	2.52	23.7 dB up to $10.6f_o$
[20]	2.4	0.16×0.11	0.78	20 dB up to $4f_o$
[21]	2.5	0.20×0.10	-	20 dB up to $2.8f_o$
This work (Fig. 13)	**2.27**	**0.35×0.035**	**1.68**	**39 dB up to $4.5f_o$ 24 dB up to $6.3f_o$**

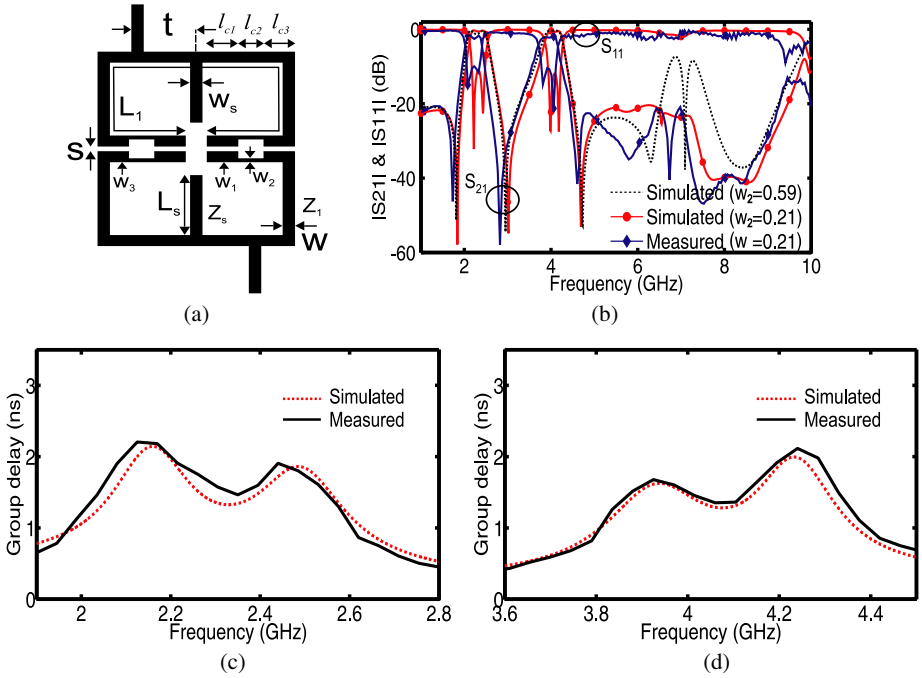

Figure 14. Dual-band BPF. (a) Layout. (b) Measured and simulated performance of the filter with third and fourth harmonic suppression. (c) First passband group delay. (d), (c) Second passband group delay.

mode analysis, the first passband f_o can be derived as:

$$f_o = \frac{c}{2L_1\sqrt{\epsilon_{eff}}} \tag{28}$$

The second passband f_1 which is due to the open-loop resonator and open-stubs can be written as:

$$f_1 = \frac{c}{(L_1 + 2L_s)\sqrt{\epsilon_{eff}}} \tag{29}$$

where c is the speed of light in free space. ϵ_{eff} stands for effective dielectric constant of the substrate. Eq. (29) is derived for the special case $Z_s = 2Z_1$. For harmonic suppression, coupled sections are changed from uniform to stepped as discussed before. The dual-band filter is designed for the frequencies $f_o = 2.24$ GHz and $f_1 = 4.02$ GHz having FBWs of 17.6% and 9.7%, respectively. Similar to the above, the quality factor and coupling-coefficient determine the tapping position t and the gap s between the resonators. The dimensions of the proposed filter are $l_{c1} = l_{c2} = 1.5$ mm, $l_{c3} = 1.27$ mm, $L_1 = 25.6$ mm,

$L_s = 3.2\,\text{mm}$, $s = 0.25\,\text{mm}$, $t = 2.7\,\text{mm}$, $w_1 = w_3 = w = 0.59\,\text{mm}$ and $w_2 = 0.21\,\text{mm}$. Fig. 14(b) shows the response of the dual-band BPF. The uniform coupled width spurious passband appears at 6.4 GHz. For $w_2 = 0.21\,\text{mm}$, the spurious passband is suppressed to $-21\,\text{dB}$ at 6.4 GHz. Also wide stopband up to 9.5 GHz has been achieved. The insertion losses at the first and second passbands are 2.45 dB and 2.1 dB, respectively. Fig. 14(c) and Fig. 14(d) plot the group delays for the two passbands. The BPF shows a group delay of less than 2.15 ns and 2.12 ns for the first and second passbands, respectively. So this technique ensures the spurious band suppression in dual-band filters without increasing the size of the filter.

8. CONCLUSION

Transmission zero behavior of two coupled-sections — interdigital and combline — has been studied. Transmission zeros are shown to be tunable with respect to the coupled width and their orientation. Further, these transmission zeros are implemented to suppress harmonics. To support the proposed idea, the second harmonic is suppressed in two parallel coupled filters based on interdigital coupling section. Also using this technique, higher-order harmonics are suppressed in open-loop filter based on combline coupled-section. The technique is also applicable to dual-band filter. All measured results are in good agreement with the simulated ones.

ACKNOWLEDGMENT

SERB, DST, India funding and reviewers' comments are profusely thanked.

REFERENCES

1. Cohn, S. B., "Parallel-coupled transmission line," *IRE Trans. Microw. Theory Tech.*, Vol. 6, 223–231, Apr. 1958.
2. Hong, J.-S. and M. J. Lancaster, "Coupling of microstrip square open-loop resonators for cross-coupled planar microwave filters," *IEEE Trans. Microw. Theory Tech.*, Vol. 44, 2099–2109, Dec. 1996.
3. Tu, W.-H. and K. Chang, "Compact microstrip bandstop filter using open stub and spurline," *IEEE Trans. Microw. Theory Tech.*, Vol. 15, 268–270, Apr. 2005.
4. Lopetegi, T., M. A. G. Laso, J. Hernandez, M. Bacaicoa, D. Benito, M. J. Garde, M. Sorolla, and M. Guglielmi, "New microstrip wiggly-line filters with spurious passband suppression," *IEEE Trans. Microw. Theory Tech.*, Vol. 49, 1593–1598, Sep. 2001.
5. Kim, B. S., J. W. Lee, and M. S. Song, "An implementation of harmonic-suppression microstrip filters with periodic grooves," *IEEE Microw. Wireless Compon. Lett.*, Vol. 14, 413–415, Sep. 2004.
6. Kim, J. K., N. Kingsley, M. Morton, R. Bairavasubramanian, J. Papapolymerou, M. M. Tentzeris, and J. G. Yook, "Fractal-shaped microstrip coupled-line bandpass filters for suppression of second harmonic," *IEEE Trans. Microw. Theory Tech.*, Vol. 53, 2943–2948, Sep. 2005.
7. Hua, W. and K. Chang, "Compact second harmonic-suppressed bandstop and bandpass filters using open stubs resonators," *IEEE Trans. Microw. Theory Tech.*, Vol. 54, 2497–2502, Jun. 2006.
8. Sanchez-Soriano, M., G. Torregrosa-Penalva, and E. Bronchalo, "Multispurious suppression in parallel-coupled line filters by means of coupling control," *IET Microwaves, Antennas & Propagation*, Vol. 6, No. 11, 1269–1276, 2012.
9. Kumar, N. and Y. K. Singh, "Compact stub-loaded open-loop bpf with enhanced stopband by introducing extra transmission zeros," *Electronics Letters*, Vol. 51, No. 2, 164–166, 2015.
10. Dai, G. L., X. Y. Zhang, C. H. Chan, Q. Xue, and M. Y. Xia, "An investigation of open- and short-ended resonators and their applications to bandpass filters," *IEEE Trans. Microw. Theory Tech.*, Vol. 57, 2203–2210, Sep. 2009.
11. Chen, C.-F., T.-Y. Huang, and R.-B. Wu, "Design of microstrip bandpass filters with multiorder spurious-mode suppression," *IEEE Trans. Microw. Theory Tech.*, Vol. 53, No. 12, 3788–3793, 2005.

12. Kim, C. H. and K. Chang, "Wide-stopband bandpass filters using asymmetric stepped-impedance resonators," *IEEE Microw. Wireless Compon. Lett.*, Vol. 23, No. 2, 69–71, 2013.
13. Kuo, J.-T., S.-P. Chen, and M. Jiang, "Parallel-coupled microstrip filters with over-coupled end stages for suppression of spurious responses," *IEEE Microw. Wireless Compon. Lett.*, Vol. 13, No. 10, 440–442, 2003.
14. Pozar, D. M., *Microwave Engineering*, 2nd Edition, Wiley, New York, 1998.
15. Hong, J.-S., *Microstrip Filters for RF/Microwave Applications*, 2nd Edition, Wiley, New York, 2011.
16. Wolfram Research, Mathematica, Version 7.0, Champaign, IL.
17. Makimoto, M. and S. Yamashita, *Microwave Resonators and Filters for Wireless Communication: Theory, Design and Application*, Vol. 4, Springer Science & Business Media, 2013.
18. Ansoft Corporation, High Frequency Structure Simulator (HFSS), Version 13.0.
19. Tsai, C.-M., S.-Y. Lee, and C.-C. Tsai, "Performance of a planar filter using a 0° feed structure," *IEEE Trans. Microw. Theory Tech.*, Vol. 50, 2362–2367, Oct. 2002.
20. Torabi, A. and K. Forooraghi, "Miniature harmonic-suppressed microstrip bandpass filter using a triple-mode stub-loaded resonator and spur lines," *IEEE Microw. Wireless Compon. Lett.*, Vol. 21, No. 5, 255–257, 2011.
21. Lin, H.-N., W.-L. Huang, and J.-L. Chen, "Miniaturization of harmonics-suppressed filter with folded loop structure," *PIERS Online*, Vol. 4, No. 2, 238–244, 2008.